Ultrasound-Modulated Two-Fluid Atomization of Dilute Polymer Solutions

Shirley C. Tsai and Patrick Luu
Dept. of Chemical Engineering, California State University, Long Beach, CA 90840

New findings presented can further our understanding of the atomization of dilute polymer solutions. First, contrary to the conventional view that viscoelastic liquids are more difficult to atomize than Newtonian liquids, it was found that aerodynamic conditions required to form uniform drops are less severe for some viscoelastic liquids than for Newtonian liquids. Under similar aerodynamic conditions, using ultrasound-modulated two-fluid atomization at 54 kHz, 40-μm-dia. uniform drops determined by the third harmonic frequency were obtained for gel-forming xantham gum solutions, but not for Newtonian liquids. Second, ultrasonic atomization yielded 350−400-μm-dia. drops for aqueous solutions of rodlike polyethylene oxides (PEO) with molecular weights of 1-2$\times 10^5$ at 54 kHz, supporting previous predictions that PEO relaxation times may be as short as 10^{-4} s. Third, at smaller molecular weights (up to 2×10^4), aqueous solutions of PEO behave like Newtonian liquids in accordance with modified Taylor's dispersion relation.

Introduction

Jet breakup by acoustic pressure waves has received considerable attention because of its application to ink-jet printing and microelectronic processing (Lang, 1962; Bogy, 1979; Elrod et al., 1989; Berger, 1991; Lal and White, 1996). The mechanism of jet breakup, however, is still not well understood. This is particularly true for non-Newtonian liquids such as polymer solutions, which are often used in jet breakup to form drops or sprays (that is, atomization). For example, in mist suppression, previous reports document that drop-size distribution broadened and peak drop diameter (the drop diameter where the peak of a drop-size distribution occurs) increased with the addition of polymers (Chao et al., 1984; Smolinski et al., 1996). Although these changes in drop size were attributed to extensional viscosity (Smolinski et al., 1996), the role of elasticity (such as elastic modulus and relaxation time) in atomization has never been empirically investigated. Furthermore, we know little about how the molecular weight and molecular structure of polymers affect the size and size distribution of atomized drops. The present study examines these phenomena using ultrasonic and ultrasound-modulated two-fluid (UMTF) atomization. UMTF atomization is a new spray technique based on amplification of ultrasound-generated capillary waves by co-flowing air (Tsai, 1997). These techniques are particularly suitable because they allow control of capillary wavelength and, therefore, of drop size (Tsai et al., 1996, 1997) and because ultrasound is often used to measure the elastic properties of materials. To date, UMTF atomization has been applied strictly to Newtonian liquids; therefore, one of the main purposes of this study is to use this technique to understand better the atomization of non-Newtonian liquids such as polymer solutions.

We found that elasticity facilitated UMTF atomization of aqueous xanthan gum solutions at an ultrasonic first harmonic frequency of 54 kHz and yielded uniform drops with a diameter (40 μm) determined by the third harmonic frequency. In addition, large drops that did not appear in the case of Newtonian liquids were obtained in ultrasonic atomization of dilute aqueous solutions of PEO with molecular weights of 1-2x10^5. At smaller molecular weights (2×10^4), aqueous PEO solutions behave like Newtonian liquids. Prior to presenting our method and findings in greater detail, we present the theoretical basis of UMTF atomization and its implications for our understanding of the jet breakup of Newtonian and polymer solutions.

Correspondence concerning this article should be addressed to S. C. Tsai: Center for Applied Science and Engineering Research, Preparatory Office (Institute of Physics) Academia Sinica, 128, Section 2, Yen Joe Yuan Road, Nanking, Taiwan 11529.

Theoretical Basis of Ultrasound-Modulated Two-Fluid (UMTF) Atomization

In UMTF atomization, a nozzle tip vibrates longitudinally at an ultrasound frequency f. As a jet of liquid with surface tension σ, kinematic viscosity ν, and density ρ issues from the nozzle tip, the ultrasound initiates on the liquid jet a capillary wave with a wavelength λ and a frequency $f/2$. The capillary wave travels axially along the jet in the direction of the airflow (X-axis) at a velocity u, where $u = \omega/k = \sqrt{2\pi\sigma/\lambda\rho}$ and λ is given (Lang, 1962; Tsai et al., 1997) by the Kelvin equation

$$\lambda = \sqrt[3]{\frac{8\pi\sigma}{\rho f^2}} \tag{1}$$

The surface elevation (or amplitude) of the resonant liquid capillary wave in the radial direction is proportional to $\cos(\omega t - kx)$ prior to air impingement. The surface elevation is amplified by the surrounding air in proportion to $\exp(\zeta t)$, where the angular frequency (velocity) $\omega = \pi f$ (Lang, 1962), the wave number $k = 2\pi/\lambda$, and ζ is the growth rate. Within the plane wave approximation, the amplitude A in the direction perpendicular to the X-axis is equal to $A_o \exp(\zeta t)\cos(\omega t - kx)$, where $x = 0$ at the nozzle tip. The initial and the boundary conditions at the nozzle tip are represented by $A = A_o\cos(kx)$ and $A = A_o\exp(\zeta t)\cos(\omega t)$, respectively. Since $t = x/u = kx/\omega$, the boundary condition can be reduced to $A = A_o\exp(\zeta kx/\omega)\cos(kx)$, which depicts an amplifying traveling wave along the X-axis. Atomization occurs when the wave amplitude is too great to maintain wave stability. The resulting peak drop diameter equals the wavelength (Tsai et al., 1996) and the jet breakup time can be calculated from the intact jet length (Tsai et al., 1999b).

The capillary wave may be treated as a plane wave when λ is much smaller than the initial radius (a) of the jet (which was the case in the present study). This allows us to use the simple linear model of temporal instability of wind-generated capillary waves first derived by Taylor (1940). Taylor's linear model was derived for viscous liquids from the equations of continuity and motion with the assumptions of irrotational liquid flow and zero tangential stress at the liquid/air interface. We modified Taylor's model by incorporating Jeffrey's hypothesis of sheltering (Jeffreys, 1925) to reduce the effects of airflow. The modified Taylor's dispersion relation is represented by the following equation (for a more detailed derivation, please see Tsai et al., 1997, 1999b)

$$\left(\zeta + 2\nu k^2\right)^2 + \frac{\sigma k^3}{\rho} - 4\nu^2 k^3\sqrt{k^2 + \zeta/\nu} - \beta\frac{\rho_A}{\rho}V_A^2 k^2 = 0 \tag{2}$$

ρ_A and V_A are air density and air velocity, respectively. Rather than closely following the troughs and crests of the capillary wave, the air current slides over the crest of one wave and impinges on the next wave (cycle) at a point between its trough and crest. Therefore, only a fraction of the wave, called the sheltering parameter β, is exposed to the airflow. β may be adjusted between zero and unity so that the relative amplitude growth rates at different wavelengths predict drop size and size distribution (Tsai et al., 1999b). β was found to account for the effect of air/liquid mass ratio (mA/mL) at a constant air velocity (Tsai et al., 1996). Note that no term in Eq. 2 includes liquid velocity, and indeed no significant effect of liquid velocity in the study ranging from 7 to 34 cm/s (Reynolds number from 6 to 300) was observed. Also note that when $\beta = 1$, Eq. 2 equals the Taylor dispersion relation, which was previously found to overestimate the amplitude growth rate (Tsai et al., 1999b).

The above theory has been used to explain the atomization of Newtonian liquids (Tsia et al., 1997; 1999a,b). The current study examines whether such a theory can be used to explain the atomization of non-Newtonian liquids such as polymer solutions.

Experimental Setup and Materials

As in our previous studies, a Malvern Particle Sizer was used for drop-size analysis in the present study. However, because the Malvern drop-size analyzer is unable to analyze drop sizes when the obscuration (fraction of laser light diffracted by the drops) falls below the minimum value of 0.02, a high-speed flow visualization system was also incorporated into the bench-scale atomization unit. The flow visualization system was also used to examine the condition of the jet exiting the atomizer. Because the experimental setup has been presented in detail elsewhere (Tsai et al., 1996, 1999b), only the UMTF atomizer, the drop-size analyzer, and the high-speed flow visualization system are described in this section.

UMTF atomizer and Malvern drop-size analyzer

As shown in Figure 1, the UMTF atomizer used in this study consists of an annulus for airflow and a Sono-Tek ultrasonic nozzle. The cross-sectional area of the annulus is adjustable to vary air velocity while maintaining a constant air-

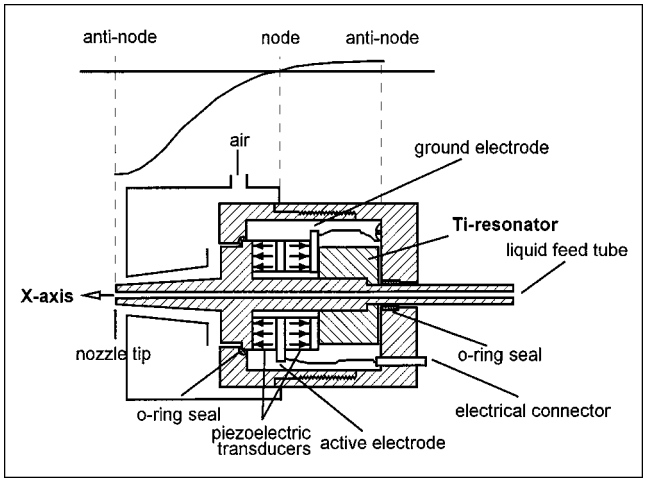

Figure 1. Cross-section view of the UMTF atomizer consisting of a Sono-Tek ultrasonic nozzle and an annulus for airflow.

Inside diameter of the liquid channel and the outside diameter of the nozzle at the tip for both nozzle No. 1 and No. 2 are 0.93 ± 0.02 mm and 2.87 mm, respectively.

to-liquid mass ratio (mA/mL). The Sono-Tek ultrasonic nozzle consists of a central tube for liquid flow, around which a pair of washer-shaped ceramic piezoelectric transducers is sandwiched between two titanium resonators located in the large diameter (about 3.6 cm) of the nozzle body. Two O-rings isolate the nozzle from the external housing. The piezoelectric transducers receive electrical input in the form of a high-frequency signal from a Sono-Tek power supply Model PS-88, and convert the input electrical energy into mechanical energy (vibration).

The nozzle is in quarter wave design. It is geometrically configured such that the excitation of the piezoelectric transducer creates a standing wave through the nozzle with maximum vibration amplitude occurring at the nozzle tip and a node at the fixed joint of the piezoelectric transducers (shown in Figure 1). Two nozzles, Model 8700-60 (nozzle No. 1) and 8700-120 (nozzle No. 2), were used in this study. For both nozzles, the outside diameter at the nozzle tip measures 2.87 mm, and the inside diameter of the liquid channel measures 0.93 ± 0.02 mm. The fundamental frequencies of the two nozzle systems are 54 kHz (nozzle No. 1) and 110 kHz (nozzle No. 2) as measured by a Hewlett Packard Spectrum Analyzer Model 8562A. The lengths of the front horn are 2.9 cm and 1.4 cm, respectively. Spectrum analyses (Tsai et al., 1996, 1997) show that the second and the third harmonics in both nozzle systems are at considerably lower power levels than the fundamental (first harmonic). The wavelengths of the capillary waves, predicted by Eq. 1, generated by the harmonics of both nozzle systems are listed in Table 1, along with the liquid properties that affect atomization of Newtonian liquids.

The Malvern Particle Sizer (Model 2600c) measures the drop sizes of the spray using diffractive scattering (Fraunhofer diffraction) of laser light. This line-of-sight measurement takes an average of 13 s of a steady-state spray. The resulting drop sizes are presented as frequency plots (vol. %) of drop diameters using a Model Independent of the Sizer software. The Particle Sizer is calibrated using a reference reticle of known particle size and size distribution. The uncertainty in drop-size measurement is $\pm 5\%$. Excellent reproducibility has been demonstrated for both UMTF atomization and ultrasonic atomization (Tsai et al., 1996, 1997). The distances between the laser beam and the nozzle tip are either 2.3 cm or 6 cm; previous findings demonstrate that the drop size and size distributions in both ultrasonic and UMTF atomization are independent of this distance (Tsai et al., 1996).

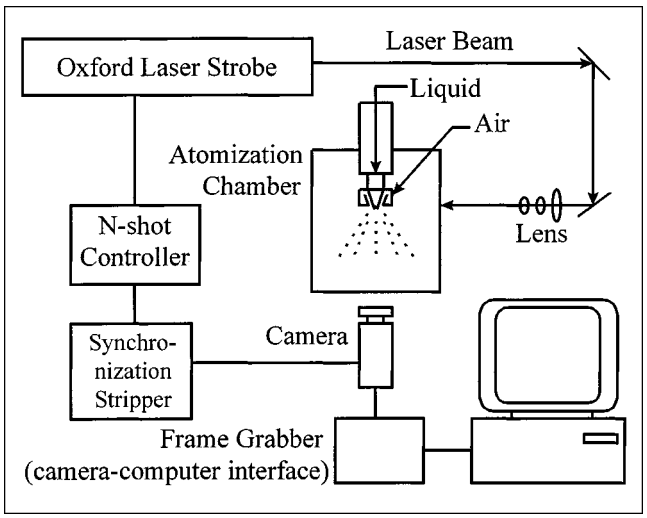

Figure 2. High-speed flow visualization system.

High-speed flow visualization system

The high-speed flow visualization system is shown in Figure 2. The System consists of an interlaced CCD video camera, light sheet optics, an Oxford copper vapor pulse laser Model CU15-A, a N-shot controller, a video synchronization stripper, a frame grabber (DT3152 by Data Translation, Inc.), and a Pentium-based computer for data acquisition and analysis using Visiflow (by AEA Technology). The CCD camera (Hitachi Denishi, Ltd., Model KP-M1U) has a 75-mm object lens. The light sheet optics consist of two mirrors, a 25-mm-lens to focus the laser beam to less than a 1-mm spot, and a cylindrical lens to expand the 1-mm beam to a light sheet 1-mm in thickness. The laser sheet is aligned along the axis of the liquid jet, and the CCD images are taken in the direction perpendicular to the laser light sheet. The copper vapor laser has 15-W power at 10,000 flashes per second. It has a pulse width (full width at half maximum intensity) of 30-nanosecond (ns) and, therefore, is capable of freezing high-speed motion. With an inter-burst period of 33 μs (30 frames

Table 1. Wavelengths of the Ultrasound-Generated Capillary Waves (in μm) Based on the Kelvin Equation

Liquid Properties			Nozzle No. 1 Ultrasounnd Freq. *f*, kHz			Nozzle No. 2 Ultrasound Freq. *f*, kHz		
σ dyne/cm	ρ g/cm^3	ν cSt	54 (1st)	168 (3rd)	282 (5th)	110 (1st)	226 (2nd)	336 (3rd)
*72	1.0	1	85	40	28	53	33	25
**62–65	1.12	5	78-79	37	26	48-49	30	23
†65	1.0	1.9 ± 0.2	82	39	27	51	32	24
‡50	1.0	1.9	76	35	25	47	29	22
§72	1.0	6.8	85	40	28	53	33	25
‖72	1.0	9.2	85	40	28	53	33	25

*Water.
**Glycerol/water mixtures with kinematic viscosity of 5 and 9.5 cSt, and respective densities of 1.12 and 1.16 g/cm^3.
†Aqueous solutions containing 0.5 wt. % and 0.75 wt. % polyethylene oxide (PEO) 10^5 molecular weight (MW) with respective kinematic viscosity of 1.7 and 2.1 cSt.
‡Aqueous solution containing 3.6 wt. % polyethylene glycol (PEG)-8000MW.
§,‖Aqueous solutions containing 0.1 wt. % and 0.15 wt. % xanthan gum (Xan), respectively.

per second), the laser strobe yields a mark space ratio of 9×10^{-4}, and the image blur is extremely low. Under illumination of such a laser strobe and combined with two 2X magnification lenses, the CCD camera is capable of imaging drops 90 μm in diameter (Tsai et al., 1999b). Although extreme care is taken to reduce reflection from the atomizer, a small bright area of the nozzle tip facing the laser light sheet is seen in the CCD images, as shown in Figure 3.

The copper vapor laser is triggered externally by the N-shot controller that operates at ''repeat single burst'' mode (mode 3). Upon receipt of an appropriate trigger pulse, the N-shot controller switches the laser off until it receives a ''laser fire'' pulse from the synchronization stripper. After receiving the ''laser-fire'' pulse, it waits for 20-ms and then fires a single burst of a selected number (one to three) of laser pulses at a 10 kHz frequency. The N-shot controller switches off the laser (time out) for 1.5 s, after which the laser reverts back to its free run frequency (9.86 kHz). When the synchronization stripper sends the ''laser-fire'' pulse to the N-shot controller, it also sends a signal to the frame grabber to synchronize the laser pulses and to the CCD camera to acquire the image. The time delays in the synchronization stripper are adjusted so that both even and odd fields of each frame are illuminated, and the frame store captures a full frame image from the CCD, which can be stored for later analysis.

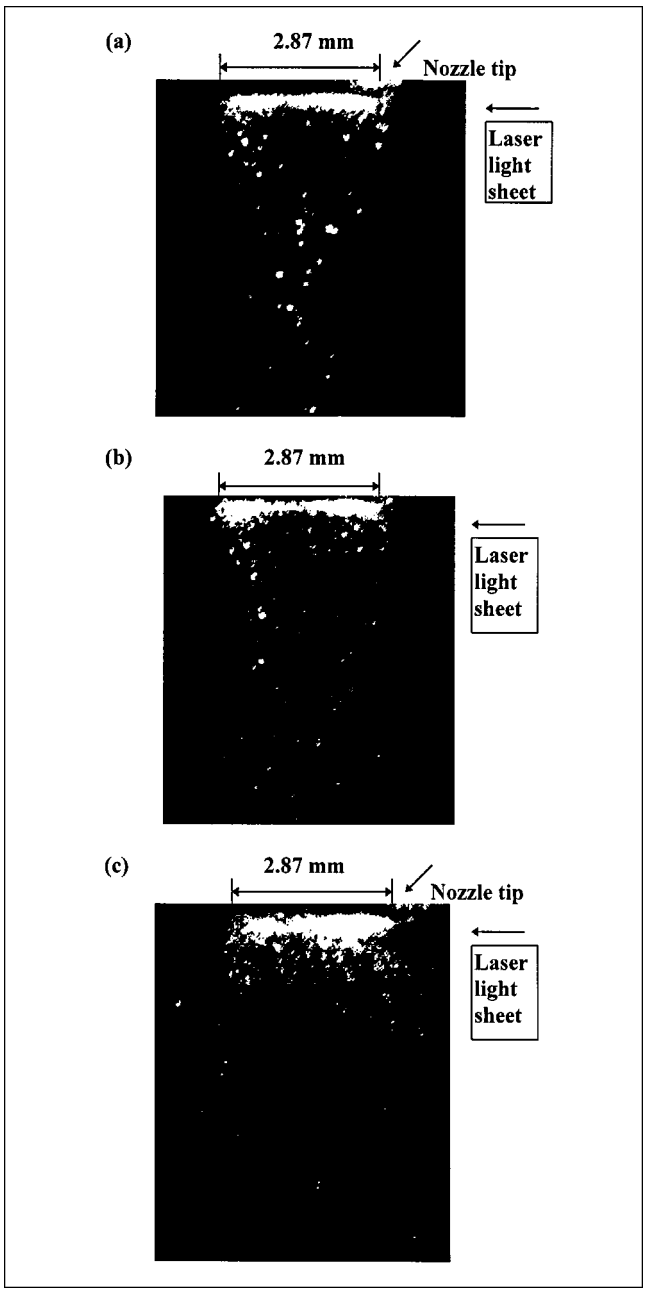

Figure 3. Flow visualization for atomization of aqueous glycerol with $\nu = 5$ cSt and $\sigma = 65 \pm 3$ dyne/cm using nozzle No. 1 at conditions.

(a) 170 m/s air velocity, 3.5 mA/mL, 2.8 W; (b) 110 m/s air velocity, 2.0 mA/mL, 2.4 W; (c) 2.7 W, without air. Note that three laser pulses are used and the OD at the nozzle tip is 2.87 mm in all three cases.

Viscoelastic properties of polymer solutions

Two structurally different water-soluble polymers were used in this atomization study: (1) polyethylene oxide (PEO) with molecular weights (MW) of 2×10^4, 10^5, 2×10^5, and 2×10^6; (2) xanthan gum (Xan, heteropolysaccharide) with MW of approximately 2×10^6. Atomization of aqueous solutions of polyethylene glycol (PEG) with 8,000 MW, Newtonian up to 43 wt. % (Dontula, 1998), was also conducted for comparison. Both PEO and Xan are reagent grades from Union Carbide. The chemical formula of PEO is $[\text{-CH}_2\text{-CH}_2\text{-O-}]_n$; the repeating unit of Xan contains five sugar units: two glucose units, two mannose units, and one glucuronic acid unit (Pal, 1995). When dissolved in water or glycerol/water mixtures, the rod-like PEO is flexible, while the Xan forms a gel and is more rigid. The viscoelastic properties of these two polymers with MW greater than 2.8×10^5 in aqueous solutions have been reported in the literature (Ortiz et al., 1994; Pal, 1995). Because of measurement limitations, however, the polymer concentrations used in these rheological studies were significantly higher than those used in the present study. Nevertheless, the available viscoelastic properties such as elastic modulus G' and characteristic time or relaxation time λ_E are summarized below to provide a description of the viscoelastic properties of the dilute polymer solutions. λ_E equals viscosity divided by elastic modulus as defined in the Maxwell Model for linear viscoelastic fluids (Bird et al., 1987).

The dimensionless elastic modulus $2G'\lambda_E/(\eta^* - \eta_S)$ is shown in Figure 4 as a function of dimensionless frequency $\lambda_E\Omega$ for aqueous polymer solutions, where η^*, η_S, and Ω are dynamic viscosity, solvent viscosity, and angular frequency, respectively. In this figure, solid circles represent data for 0.167 wt. % Xan in water (Pal, 1995) and solid diamonds for 1–3 wt. % PEO (1.8×10^6 MW) in water and glycerol/water 50 wt. % mixtures (Ortiz et al., 1994). As demonstrated in Figure 4, the former solution is more elastic than the latter solution. It should be noted that the PEO concentration from 1 to 3 wt. % and solvent viscosity from 1 mPa·s (water) to 5.4 mPa·s (50 wt. % glycerol in water) have no effect on the relationship between $2G'\lambda_E/(\eta^* - \eta_S)$ and $\lambda_E\ \Omega$ (Ortiz et al., 1994). Furthermore, as seen in Table 2, the elastic modulus G' at 1 s^{-1} and the relaxation time λ_E of

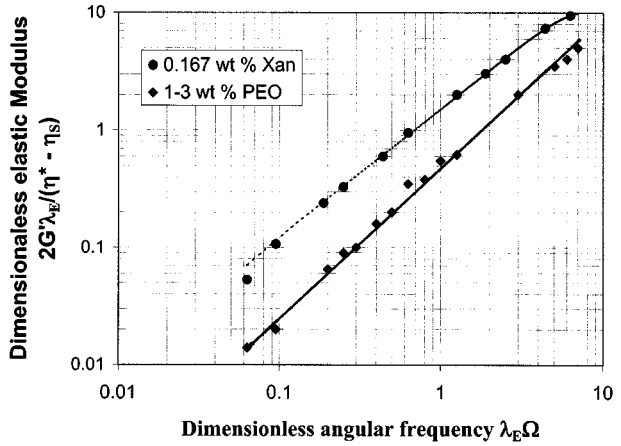

Figure 4. Dimensionless plot of elastic modulus G′ and characteristic time λ_E vs. angular frequency Ω of PEO (1.8×10^6 MW) solutions (1–3 wt. % in glycerol/water with ν = 5 cSt and 3 wt. % in water) and 0.167 wt. % Xan (2×10^6 MW) solution.

η^* and η_S are dynamic viscosity and solvent viscosity, respectively.

0.167 wt. % Xan in water are significantly greater (0.3 vs. 0.1 Pa and 1.0 vs. 0.01 s, respectively) than those of 1 wt. % PEO in water. Thus, aqueous Xan solutions are more elastic than aqueous PEO solutions, even when they are one order of magnitude lower in concentration. These reported results are consistent with our observations during the sample preparations: Xan molecules in water form gel but the PEO molecules do not. The gelation of Xan solutions may be attributed to intermolecular hydrogen bonding (Peng and Landel, 1981).

In addition to the characteristic times (λ_E) of the 0.167 wt. % Xan and 0.5–1.0 wt. % PEO solutions, Table 2 also lists the relaxation times λ_k associated with relaxation strengths G_k for dilute solutions of PEO-4×10^6 MW. Four pairs of (λ_k, G_k) were found to be required when the experimental elastic and viscous moduli G′ and G″ were simultaneously fitted to a series of Maxwell elements using nonlinear regression (Dontula et al., 1998). Although the shortest predicted relaxation time is on the order of 5×10^{-4} s, this has never been experimentally verified because moduli cannot be measured at high frequencies (Dontula et al., 1998). However, the ultrasonic atomization results reported in this article may provide empirical support of the predicted relaxation time, as will be described in the Results and Discussion section.

Preparation of polymer solutions

Dilute polymer solutions used in this study were prepared by dissolving a weighed amount of polymer in de-ionized water in a sonic bath followed by dilution to 2-L solution. The diluted solution was stirred for five hours using a 2-in. (5 cm) bar magnet to ensure solution homogeneity. The surface tension and the viscosity of the resulting solutions were measured by a ring-type surface tensiometer (Fisher Model A100) and a Cannon/Fenske tube viscometer. As shown in Table 1, these polymer solutions have surface tensions and low shear viscosity comparable to those of Newtonian liquids. Since the shear rate at which the viscosity (low shear viscosity) was measured may differ from the shear rate under atomization conditions, we also measured the flow rates of the polymer solutions. The calibration curves of the flow rates are compared with those of Newtonian liquids with known viscosity (2, 5.6, and 11 cP or mPa·s) in Figure 5. This figure shows that within the studied flow rates of 3–14 cc/min, the viscosity of the 0.75 wt. % PEO-10^5 MW solution coincides with that of the Newtonian liquids with a viscosity of 2 mPa·s, while the viscosity of the 0.5 wt. % PEO-10^5 MW solution is smaller. The viscosities of the 0.1–0.15 wt. % Xan solutions lie between 5.6 and 11 mPa·s(cP). Note that the viscosities of 5.6 and 11 mPa·s are equivalent to 5 and 9.5 cSt for aqueous glycerol solutions with respective densities of 1,120 and 1,160 kg/m^3. Moreover, it should be pointed out that the shear viscosity of aqueous glycerol solutions containing 0.8 wt. %

Table 2. Elastic Modulus G' at shear rate 1 s^{-1} and Characteristic Time λ_E, Relaxation Strength G_k and Relaxation Time λ_k for Aqueous Solutions of Xanthan Gum (Xan) and Polyethylene Oxide (PEO)

Solvent, wt. % Viscosity η_s	Polymer Conc., Zero Shear Viscosity η_o Except*	G', Pa @ 1 s^{-1}	G_k, Pa	λ_E or λ_k, s	Ref.
Water 0.001 Pa·s	0.5 wt. % PEO-2×10^6 MW 0.02 Pa·s			0.01	Ortiz et al. (1994)
Water 0.001 Pa·s	1.0 wt. % PEO-1.8×10^6 MW 0.14 Pa·s	0.1		0.01	Ortiz et al. (1994)
38% PEG-8000 0.134 Pa·s	0.08 wt. % PEO-4×10^6 MW 0.185 Pa·s* @ 1 s^{-1}	10^{-2}	265.1 2.7×10^{-1} 3.0×10^{-2} 6.6×10^{-4}	5.1×10^{-4} 7.2×10^{-2} 6.2×10^{-1} 7.83	Dontula et al. (1998)
38% PEG-8000 0.134 Pa·s	0.06 wt. % PEO-4×10^6 MW 0.151 Pa·s* @ 40 s^{-1}	4×10^{-3}	221.5 1.2×10^{-1} 1.7×10^{-2} 9.5×10^{-4}	5.7×10^{-4} 7.9×10^{-2} 4.6×10^{-1} 4.79	Dontula et al. (1998)
Water 0.001 Pa·s	0.167% Xan-2×10^6 MW 1.8 Pa·s**	0.3		1.0	Pal (1995)

*Steady shear viscosity (Newtonian at shear rates from about 0.2 s^{-1} up to values given).
**Steady shear viscosity η (in Pa·s) = 0.35 $\gamma^{-0.67}$ at shear rates γ from 1 to 200 s^{-1}.

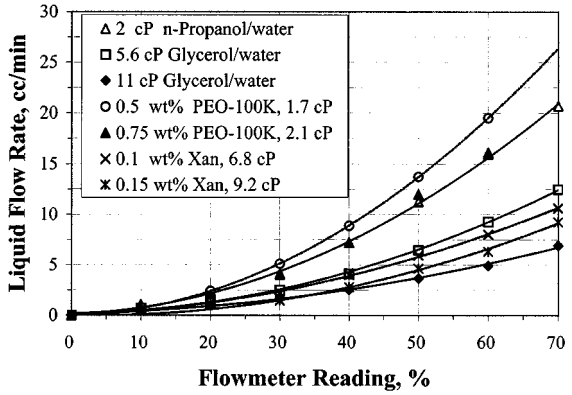

Figure 5. Calibration curves of the Brooks precision rotameter.

Note that 1 cP = 1 mPa·s, and 1 cP equals density in g/cm^3 multiplied by kinematic viscosity ν in cSt.

PEO-10^5 MW was found to remain constant (5 mPa·s) at shear rates from 20 to 1,000 s^{-1} (Munn et al., 1999). The Trouton ratio (extensional viscosity divided by steady shear viscosity) was also found equal to the Newtonian value of 3 (Munn et al., 1999).

Atomization of the Newtonian aqueous glycerol (or n-propanol) solutions with 2 cSt kinematic viscosity has been reported elsewhere (Tsai et al., 1999a). Therefore, only atomization of the Newtonian aqueous glycerol solutions with kinematic viscosity 5 and 9.5 cSt is reported in this article as a comparison for the dilute polymer solutions.

Results and Discussion

The following section is divided into three parts. First, we demonstrate the initiation of capillary waves as assumed in the theory described above for Newtonian and non-Newtonian liquids. Second, we compare the relative amplitude growth rates of the capillary waves at different wavelengths to drop size and size distributions for Newtonian and non-Newtonian liquids. We show that with molecular weights up to 2×10^4, PEO solutions show Newtonian behavior in accordance with the predictions of modified Taylor's dispersion curves; however, with molecular weights greater than 10^5, PEO solutions develop drops that Newtonian liquids do not. Third, elasticity is shown to facilitate UMTF atomization of gel-forming xanthan gum solutions.

Initiation of capillary waves

Figures 3 and 6 are flow visualizations of the sprays of glycerol/water mixture ($\sigma = 65\pm3$ dyne/cm, $\nu = 5$ cSt) near the nozzle tip. These pictures were taken using a CCD camera from the direction perpendicular to the incident light sheet that is generated by an Oxford 30-ns pulsed laser (in three pulses). Figures 3a and 3b show bright bands 2.87-mm wide in UMTF atomization using nozzle No. 1 at two conditions (air velocities of 174 and 110 m/s, air-to-liquid mass ratios of 3.5 and 2.0, and ultrasonic power levels of 2.8 and 2.4 W, respectively). A bright band is also seen in Figure 3c for ultrasonic atomization at 2.7 W (without air). The bright band covers the entire outside diameter (2.87 mm) of the nozzle tip; this diameter serves as a reference linear scale. Bright spots below the bright band in Figures 3a and 3b are due to light scattering and represent clusters of drops 40 μm in diameter. The bright spots or clusters of drops are larger and more focused in Figure 3a than those in Figure 3b because of the higher air velocity (174 vs. 110 m/s) in the former figure. Individual drop sizes are 40 μm in diameter, as seen in Figure 7; however, they are too small to be seen in Figures 3a and 3b because the lens can only capture drop sizes greater than or equal to 90 μm.

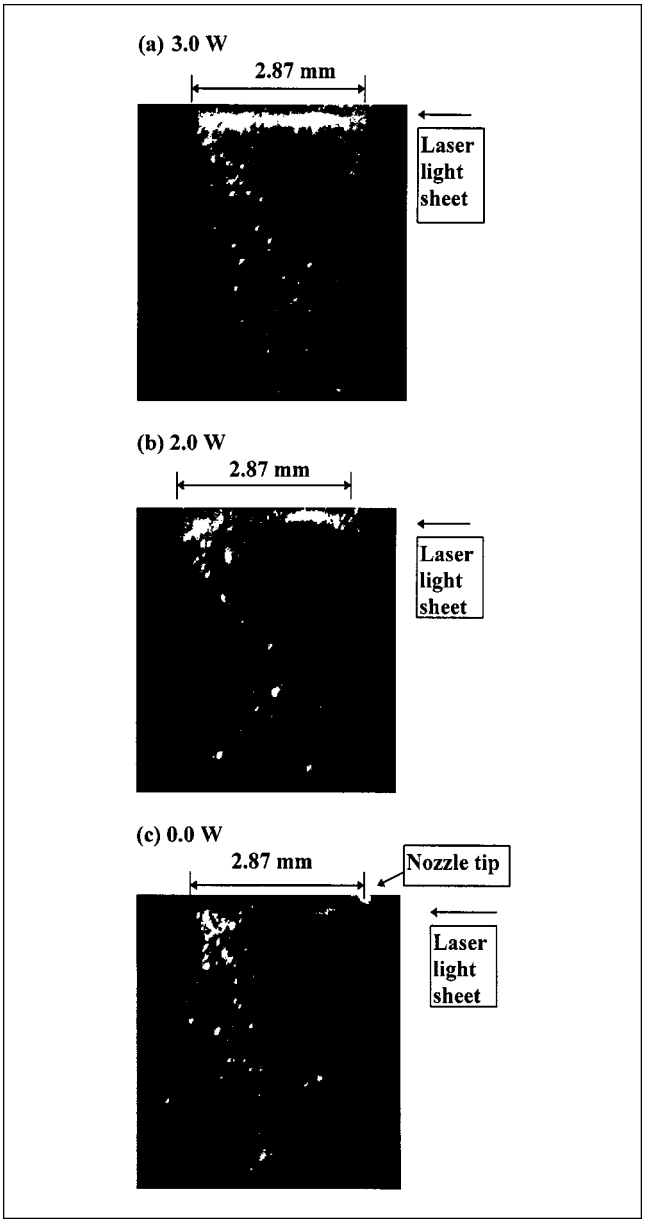

Figure 6. Flow visualization of UMTF atomization of 5.5 cc/min glycerol/water mixture with $\nu = 5$ cSt and $\sigma = 65\pm3$ dyne/cm at 170 m/s air velocity and 3.5 mA/mL at various ultrasonic power levels using nozzle No. 1 (54 kHz) with 2.87 mm OD at the nozzle tip.

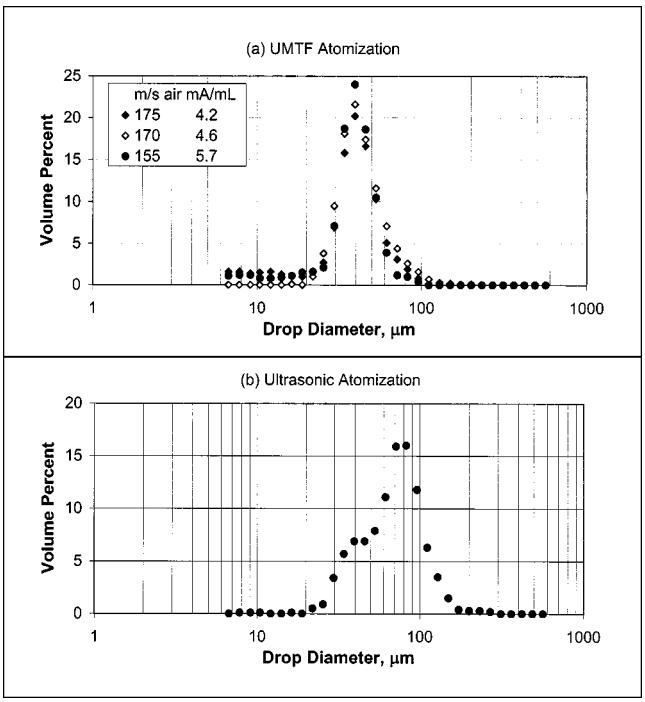

Figure 7. Drop-size distributions for 5.5 cc/min aqueous glycerol with $\nu = 5$ cSt and $\sigma = 65 \pm 3$ dyne/cm.

(a) UMTF atomization at 2.5 W; (b) ultrasonic atomization at 2.5 W using nozzle No. 1 (54 kHz).

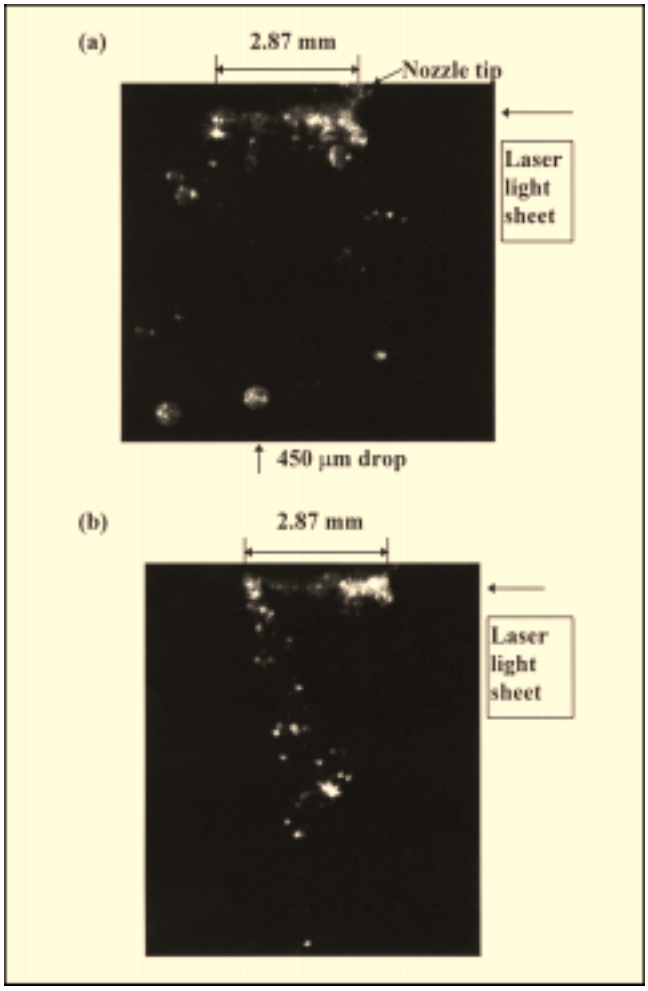

Figure 8. Flow visualization for 6.8 cc/min aqueous solution of 0.5 wt. % PEO-10^5 MW ($\sigma = 65$ dyne/cm and $\nu = 1.7$ cSt).

(a) Ultrasonic atomization at 2.5 W; (b) UMTF atomization at 145 m/s air velocity, 2.8 mA/mL, 2.5 W (b) both using nozzle No. 1 (54 kHz) with 2.87 mm OD at the nozzle tip.

The band becomes weaker as the ultrasonic power level decreases from 3.0 W to 2.0 W (compare Figure 6a and 6b). We believe that the observed band is due to scattering of the laser light by the capillary waves (ripples) generated by the ultrasound. Indeed, no such band is seen in two-fluid atomization without ultrasound (see Figure 6c, 0.0 W). We observed a clear liquid jet facing the incident light sheet, which is black in the photo (see righthand side of Figure 6c) due to the lack of light scattering (no ripples). Furthermore, a bright wavy band near the nozzle tip is seen in Figure 8 for both the ultrasonic and UMTF atomization of dilute aqueous solution of PEO-10^5 MW. The band is also due to scattered light from the ultrasound-generated capillary waves. No bright band was seen in two-fluid (without ultrasound) atomization of the same PEO solution. Thus, the initiation of capillary waves by ultrasound at the nozzle tip is verified.

Relative amplitude growth rates of the capillary waves

The dispersion curves based on Eq. 2 at 170 m/s air velocity for water ($\sigma = 72$ dyn/cm; $\nu = 1$ cSt) and glycerol-water mixtures with $\sigma = 62$ dyne/cm, $\nu = 2$, 5, and 9.5 cSt are shown in Figure 9. In the figure, wave number k is nondimensionalized by the initial radius (a) of the jet. As shown in Figure 9, the modified model predicts that the amplitude growth rate decreases as the liquid viscosity increases. The predicted wavelength of the capillary wave with maximum growth rate becomes longer as the sheltering parameter β decreases. For example, the wavelength with maximum growth rate shifts from 22 μm to 28 μm as β decreases from unity to 0.7–0.8 for the 5 cSt liquid. Nevertheless, at β ranging from 0.7 to 1.0, the amplitude growth rate is significantly greater for the 40-μm wave than for the 80-μm wave. The very narrow drop-size distribution with a single peak at 40 μm drop diameter shown in Figure 7a for UMTF atomization of the 5 cSt aqueous glycerol solution using nozzle No. 1 (54 kHz) is consistent with theoretical predictions. The 40- and 80-μm drops (see the drop-size distribution in Figure 7b) result from the breakup of the capillary waves about 40 and 80 μm in wavelength, which are generated by the third and the first harmonics of the ultrasound, respectively.

In contrast, Figure 9 shows that the predicted amplitude growth rate for the 23 μm-wave on liquid medium with $\nu = 5$ cSt is comparable to that of 50 μm-wave at $\beta = 0.7$ or 0.8. However, at $\beta = 1.0$, the predicted amplitude growth rate for the 23 μm-wave is significantly greater than that of the 50 μm-wave. UMTF atomization of the 5 cSt aqueous glycerol at 170 m/s air, 7.2 mA/mL, and 2.9 W using nozzle No. 2 (110 kHz ultrasound fundamental frequency) yielded a bi-

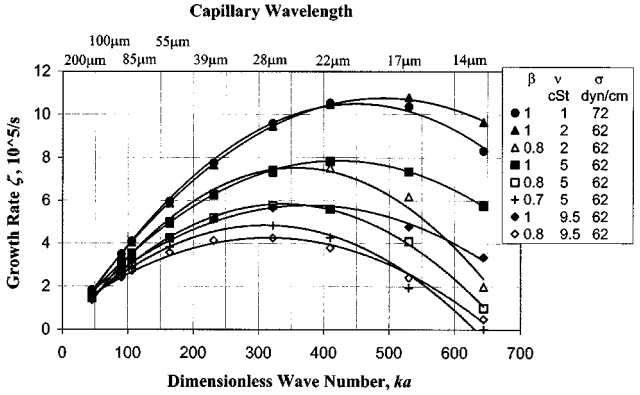

Figure 9. Taylor's and modified Taylor's dispersion curves of amplitude growth rates ζ for water (σ = 72 dyn/cm and ν = 1 cSt) and liquids with σ = 62 dyne/cm and ν = 5 and 9.5 cSt at 170 m/s air velocity.

β and a are sheltering parameter and initial jet radius, respectively; $2a = 2.87$ mm.

modal drop-size distribution with a primary peak at 20 μm and a secondary peak around 50 μm. Therefore, the experimental results are in better agreement with the theoretical predictions at $\beta = 0.7$ or 0.8 than those at $\beta = 1.0$. The 23 and 50 μm waves are generated by the third and the first harmonics of the ultrasonic nozzle No. 2 system. Likewise, the multiple-peak drop-size distributions shown in Figure 10 for UMTF atomization of aqueous glycerol with $\sigma = 62$ dyne/cm and $\nu = 9.5$ cSt at 170 m/s air velocity using nozzle No. 1 are also consistent with the comparable amplitude growth rates at $\beta = 0.8$ predicted in Figure 9 for this liquid. This is also true for UMTF atomization of the glycerol/water mixture with $\sigma = 62$ dyne/cm and $\nu = 5$ cSt at a lower air velocity (145 m/s) using nozzle No. 1; the resulting drop-size distribution is shown in Figure 10.

Aqueous PEO Solutions with Molecular Weights $\leq 2 \times 10^4$. The kinematic viscosity and the surface tension of aqueous solutions of 3.5—3.6 wt. % PEG-8000 MW and PEO-2×10^4 MW are 2.0 ± 0.2 cSt and 47-50 dyne/cm, respectively. Ultrasonic atomization and UMTF atomization of these solutions

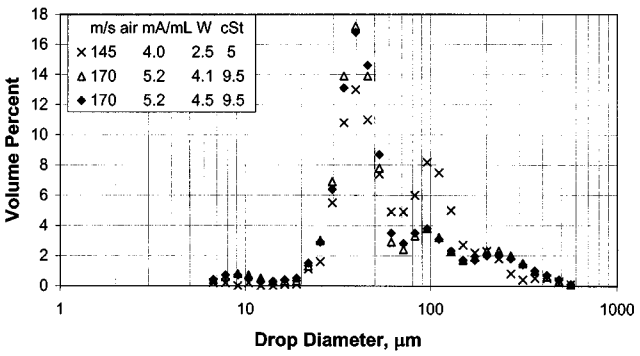

Figure 10. Drop-size distributions of UMTF atomization of aqueous glycerol with σ = 62 dyne/cm and ν = 5 and 9.5 cSt at liquid flow rates of 3.6–4.2 cc/min using nozzle No. 1.

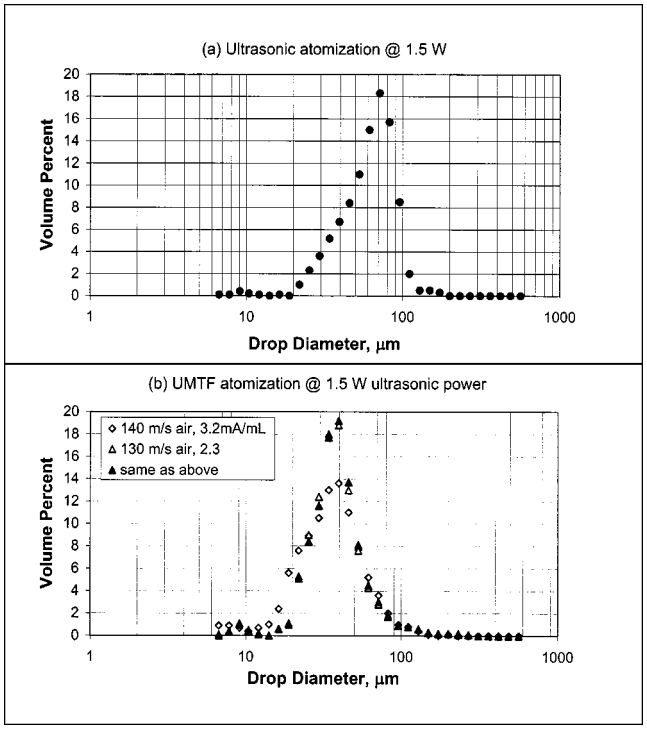

Figure 11. Drop-size distributions for aqueous 3.6 wt. % PEG-8000 MW solution (σ = 50 dyne/cm and ν = 1.9 cSt) at liquid flow rates 6–8 cc/min.

(a) Ultrasonic atomization at 1.5 W; (b) UMTF atomization at 1.5 W, both using nozzle No. 1 (54 kHz).

yielded drop-size and size distributions similar to those of Newtonian liquids with similar surface tension and viscosity (Tsai et al., 1999a). For example, ultrasonic atomization of an aqueous solution containing 3.6 wt. % PEG-8000 using nozzle No. 1 (54 kHz) at 1.5 W gives rise to a drop-size distribution with a primary peak at 70 μm and a tail extending to 20 μm (see Figure 11a). In contrast, a peak around 35 μm-diameter is seen in the drop-size distribution as shown in Figure 11b when air at 130−140 m/s and 2.3−3.2 mA/mL is added. The vol. % of the 70-μm diameter is very small. The 70-μm and 35-μm drops are generated by the first and the third harmonic of the ultrasound. The dominance of the 35 μm drops is consistent with the much greater amplitude growth rate for the 35 μm-wave than that of the 70 μm wave predicted by Eq. 2 at this aerodynamic condition.

Likewise, UMTF atomization of the PEG-8000 solution at 95-110 m/s air velocity and 2.7−3.1 mA/mL using nozzle No. 2 (110 kHz) at 3.5 W ultrasonic power was found to yield a peak at 35 μm-diameter because the amplitudes of the 47-μm and 22-μm waves grew at equal rates. The 22 μm-diameter peak was found to dominate over the 47 μm-diameter peak as the air velocity increased to 140−160 m/s because the 22 μm-waves grew at a higher rate than the 47-μm wave. Note that the capillary waves 47 μm and 22 μm in wavelength were generated by the first and the third harmonics of nozzle No. 2, respectively (see Table 1). The power inputs to the ultrasonic nozzles required in either ultrasonic or UMTF atomization were also about the sames as the those for Newto-

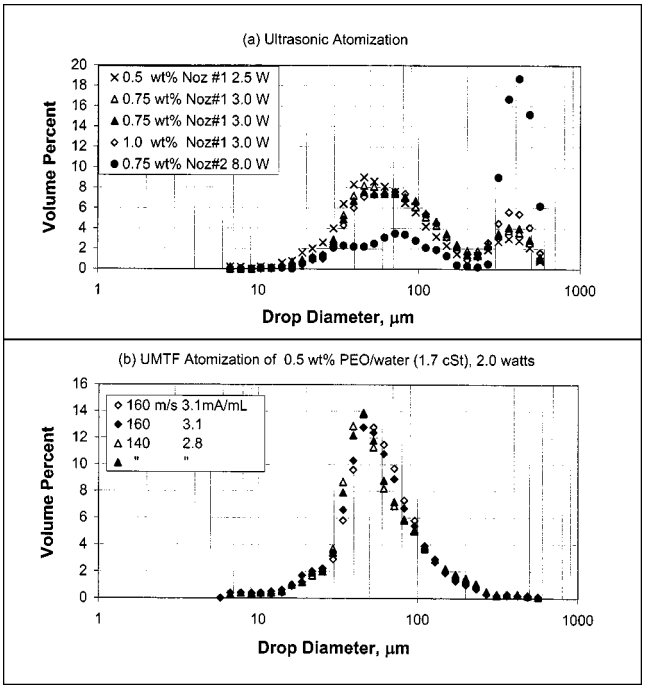

Figure 12. Drop-size distributions for aqueous PEO-10^5 MW solutions of 0.5–0.75 wt. % ($\sigma = 62 \pm 3$ dyne/cm and $\nu = 1.9 \pm 0.2$ cSt) at 5.5–6.7 cc/min and 1.0 wt. % ($\sigma = 66$ dyne/cm and $\nu = 2.5$ cSt) at 3.7 cm^3/min.

(a) Ultrasonic atomization; (b) UMTF atomization at 2.0 W, both using nozzle No. 1 (54 kHz).

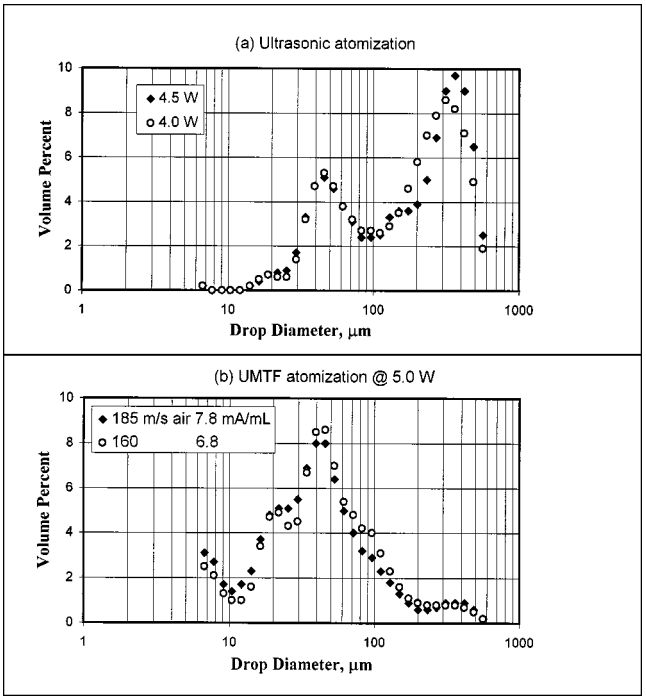

Figure 13. Drop-size distributions for 3 cc/min aqueous PEO-2×10^5 MW solution ($\sigma = 57$ dyne/cm and $\nu = 2.2$ cSt).

(a) Ultrasonic atomization at 4.0–4.5 W; (b) UMTF atomization at 5.0 W using nozzle No. 1 (54 kHz).

nian liquids. Once above a threshold value, the ultrasonic power input at a fixed ultrasonic frequency was found to have no significant effect on the drop-size and size distribution in both ultrasonic and UMTF atomization.

Thus, aqueous solutions of PEO with molecular weights 2×10^4 and lower behave like Newtonian liquids in both ultrasonic and UMTF atomization. The drop-size and size distribution is predicted by Eq. 2, the modified Taylor's dispersion relation. The peak drop diameter is determined by the ultrasonic frequency f in accordance with Eq. 1, the Kelvin equation with $f^{-2/3}$-dependency.

PEO Solutions with Molecular Weights $\geq 10^5$. PEO solutions with molecular weights $\geq 10^5$ were found to require more ultrasonic power than the Newtonian liquids described above for both ultrasonic and UMTF atomization. However, for PEO solutions, the effects of molecular weight on drop-size distribution differed significantly for the two techniques. As shown in Figure 12a, ultrasonic atomization of aqueous solutions of 0.5–0.75 wt. % PEO-10^5 MW ($\sigma = 62 \pm 3$ dyne/cm and $\nu = 1.9 \pm 0.2$ cSt) at an ultrasonic fundamental frequency of 54 kHz (nozzle No. 1) and an ultrasonic power of 2.5–3.0 W yields a very broad drop-size distribution. This drop-size distribution covers the drop diameters 82 and 40 μm, which are generated by the first and third harmonics based on Eq. 1. More importantly, new drops as large as 400 ± 25 μm in diameter also appear in Figure 12a. This figure also shows that the percentage of large drops becomes greater as the PEO-10^5 MW concentration increases to 1.0 wt. % ($\sigma = 66$ dyne/cm and $\nu = 2.5$ cSt). As seen in Figure 8a, large drops are also formed in ultrasonic atomization of 0.5 wt. % PEO-10^5 MW solution using nozzle No. 1. Figure 12a shows that the 400-μm peak predominates when the ultrasonic frequency increases from 54 to 110 kHz (nozzle No. 2); the threshold ultrasonic power required for atomization to occur also increases from 3.0 W to 8.0 W. The percentages of the drops (53–25 μm) generated by the harmonics of the ultrasound are small. No large drops 400 ± 25 μm in diameter were observed in two-fluid atomization (without ultrasound) of aqueous solutions of PEO-10^5 MW at 140–160 m/s air velocity.

A predominance of large drops (350 ± 50 μm) is also observed in Figure 13a for ultrasonic atomization at ultrasonic power levels of 4.0 W and above, using nozzle No. 1 for the PEO-2×10^5 MW solution. This solution has similar surface tension (57 dyne/cm) and viscosity (2.2 mPa·s) as the PEO-10^5 MW solutions in Figures 8 and 12.

The large drops (approximately 400 μm in diameter) may be due to the breakup of the capillary wave with a frequency of about 5 kHz (wavelength of 400 μm based on Eq. 1), which is one order of magnitude lower than the first harmonic frequency (54 kHz) of nozzle No. 1. The 5 kHz capillary wave with a cycle time of 2×10^{-4} s is due to molecular motion, such as change in the configuration of the rod-like PEO polymer. As shown in Table 2, relaxation time as short as 5×10^{-4} s has been predicted for PEO with MW of 4×10^6 (Dontula et al., 1998). Therefore, we believe that the ultrasonic energy sets up the PEO molecular motion and relaxation, resulting in the 5 kHz capillary wave, which breaks up into drops ap-

proximately 400 μm in diameter when its amplitude becomes too great to maintain wave stability.

Further increase in PEO molecular weight to 2×10^6 resulted in no atomization even when PEO concentration was as low as 0.07 wt. % ($\nu = 1.9$ cSt). Since the obscuration fell below the detection limit of the Malvern drop-size analyzer, flow visualization using the Oxford 30 ns-pulse laser was carried out to examine the jet breakup with nozzle No. 1. No atomization occurred at 6.0 W ultrasonic power. However, drops as large as 1.6 mm in diameter were found at 8.0 W without air; the diameter of these drops was larger than the inside diameter (0.93 mm) of the nozzle at the tip. These large drops may be due to Rayleigh-mode jet breakup (Bousfield et al., 1986), which involves a time scale on the order of seconds.

In contrast, a significant amount of large drops beyond the predictions of Eq. 1 was not found in the UMTF atomization of aqueous solutions of PEO with molecular weights $10^5-2\times10^6$ using nozzle No. 1. Specifically, no 400 μm-diameter drops are seen in Figures 12b and 8b in UMTF atomization of 0.5 wt. % aqueous solution of PEO-10^5 MW at air velocity from 140 to 160 m/s, mA/mL from 2.8 to 3.1, 54 kHz ultrasonic frequency and 2.0 W power. In fact, a careful comparison of Figure 12b to Figure 11b reveals only minor differences. The drop-size distribution for the PEO-10^5 MW solution is broader (half-width of 45 vs. 35 μm), because the vol. % of the drops approximately 80 μm in diameter is greater (6.5 vs. 2.0%) in Figure 12b than in Figure 11b. The peak diameter is slightly larger (45 vs. 40 μm), and the threshold ultrasonic power requirement is slightly higher (2.0 vs. 1.5 W) for the PEO-10^5 MW solution than for the Newtonian PEG-8000 solution. The ultrasonic power requirement becomes much greater (5.0 vs. 2.0 W) and the drop-size distribution becomes much broader (compare Figure 13b to 12b) in UMTF atomization as the PEO molecular weight increases from 10^5 to 2×10^5. Nevertheless, the peak diameter remains at 45 μm, and the vol. % of the 400 μm drops is very small. As for the PEO-10^5 MW solution, no 400 μm drops were obtained when air at 105 m/s velocity and 2.2 mA/mL was introduced in combination with ultrasound at 54 kHz and 6.0 W to the jet of PEO-2×10^6 MW solution.

Furthermore, no 400 μm drops were obtained in UMTF atomization of the aqueous solution of 0.75 wt. % PEO-10^5 MW using nozzle No. 2 (110 kHz fundamental frequency) even though these drops predominate in ultrasonic (without air) atomization, as shown in Figure 12a. In fact, the drop-size distribution showed two peaks of 9% each at 80-μm and 40-μm diameter and a shoulder peak of 2.5 % at 15-μm diameter when the required conditions were 140–160 m/s air velocity, 4.1–5.6 mA/mL, and 5.0 W ultrasonic power. These three peaks were also found in two-fluid atomization (without ultrasound) of this solution at the same aerodynamic conditions; the vol. % were 10%, 7%, and 4% for the 80 μm-, 40 μm, and 15 μm-diameter, respectively.

In summary, the capillary wave generated by the third harmonic (174 kHz frequency) of the ultrasound grows at a greater rate than the longer waves in UMTF atomization of aqueous solutions of PEO with molecular weights on the order of 10^5 using nozzle No. 1 (54 kHz fundamental frequency). The longer waves include the capillary wave generated by the first harmonic and the 400 μm-wave resulting from the PEO molecular relaxation. Increase in ultrasonic fundamental frequency from 54 to 110 kHz yields no reduction in drop sizes, which is contrary to the Newtonian behavior of $f^{-2/3}$-dependency. In addition, as the PEO molecular weight increases, the growth rates of the capillary waves generated by the harmonic of the ultrasound become more comparable and the drop-size distributions become broader. Eventually, the Taylor-mode breakup of capillary waves in ultrasonic atomization of aqueous solutions of PEO-2×10^{-6} MW gives way to Rayleigh-mode jet breakup that creates drops of a diameter larger than the initial jet diameter.

Elasticity facilitates UTMF atomization

Increase in Xan concentration from 0.1 wt. % to 0.15 wt. % results in an increase in kinematic viscosity from 6.8 to 9.2 cSt, but does not change the surface tension (72 dyne/cm) or density (1.0 g/cm^3). This increase in viscosity leads to increased ultrasonic power requirements from 3.5 to 4.5 W in ultrasonic atomization using nozzle No. 1 (54 kHz) and from 2.5 to 3.5 W in UMTF atomization also using nozzle No. 1. Nevertheless, the drop-size distribution remain unchanged, as shown in Figure 14.

A comparison of Figure 14a and Figure 7a shows that the power requirement (2.5 W) and the peak drop diameter (40 μm) for the 0.1 wt. % Xan solution and the Newtonian aqueous glycerol are the same. More importantly, the required air velocity (100 vs. 155 m/s) and air-to-liquid mass ratio (3.3 vs. 5.7 mA/mL) are significantly smaller for the aqueous Xan solution than for the aqueous glycerol. The latter was found to be stable at the less severe aerodynamic conditions (100

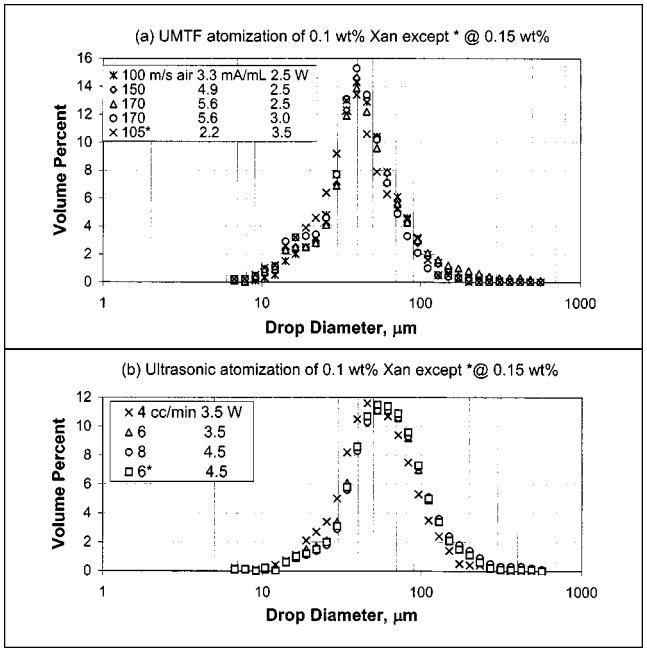

Figure 14. Drop-size distributions for 0.1 wt. % Xan solution (σ = 72 dyne/cm and ν = 6.8 cSt) and 0.15 wt. % Xan solution (σ = 72 dyne/cm and ν = 9.2 cSt) at flow rates of 4–6 cm^3/min,

(a) UMTF atomization; (b) ultrasonic atomization using nozzle No. 1 (54 kHz).

m/s air velocity and 3.3 mA/mL) under which the former atomized. As shown in Figure 10, the Newtonian aqueous glycerol jet yields multiple peaks in UMTF atomization at even more severe aerodynamic conditions (145 m/s air velocity and 4.0 mA/mL). Likewise, Figure 14a shows that UMTF atomization of 0.15 wt. % Xan solution ($\sigma = 72$ dyne/cm and $\nu = 9.2$ cSt) yields a drop-size distribution with single peak at 40 μm-diameter, while that of the Newtonian aqueous glycerol ($\sigma = 62$ dyne/cm and $\nu = 9.5$ cSt) yields multiple peaks (as shown in Figure 10). The atomization conditions are 105 m/s air velocity, 2.2 mA/mL, and 3.5 W for the Xan solution; they are much more severe (170 m/s air velocity, 5.2 mA/mL, and 4.5 W) for the aqueous glycerol. At the aerodynamic conditions of 105 m/s air velocity and 2.2 mA/mL without ultrasound, neither the 0.15 wt. % Xan solution nor the aqueous glycerol ($\nu = 9.5$ cSt) atomized.

Furthermore, a comparison of Figure 14b with Figure 7b reveals that the power requirement for ultrasonic atomization of the 0.1 wt. % Xan solution is significantly higher (3.5 W vs. 2.5 W) than that of the aqueous glycerol with $\nu = 5$ cSt. The power requirement in ultrasonic atomization of the 0.15 wt. % Xan solution was found to be the same (4.5 W) as that of the aqueous glycerol with $\nu = 9.5$ cSt. These ultrasonic atomization results suggest that the Xan solutions are by no means less viscous, under the shear conditions of atomization, than their Newtonian counterparts. In fact, the viscosity curves of the 0.1–0.15 wt. % Xan solutions lie between 5.6 mPa·s (5 cSt) and 11 mPa·s (9.5 cSt) at all flow rates used in this atomization study, as shown in Figure 5. In addition, a careful comparison of Figure 14b with Figure 7b also reveals that the ratio of the two peaks at 40-μm and the 85-μm drop diameters is significantly greater (1 vs. 1/3) for the Xan solutions than for the Newtonian aqueous glycerol. (The ultrasonic power from 2.5 to 4.5 W was found to have no significant effect on this ratio in ultrasonic atomization of the aqueous glycerol.) Therefore, the initial condition for the 40-μm wave to dominate in UMTF atomization is more favorable for the Xan solutions than for the Newtonian liquids. Upon air impingement, the amplitude of the 40-μm capillary wave becomes too great to maintain wave stability, resulting in uniform drops 40-μm in diameter. Consequently, the required aerodynamic conditions are less severe for the Xan solutions than for the Newtonian liquids.

Based on the above technical considerations, the ease with which the UMTF atomization of Xan solutions yields uniform drops 40-μm in diameter contradicts the detrimental effects of viscosity. We believe this ease is due to elasticity, because the xanthan gum molecules are interconnected to form a network in the solution (like gel) via intermolecular hydrogen bonding. As discussed previously, the dilute gel-forming Xan solutions are more elastic than the dilute rod-like PEO solutions in which no intermolecular hydrogen bonding is possible. Accordingly, as shown in Figure 14a, the Xan solutions with a kinematic viscosity of 9.2 cSt yield uniform drops 40-μm in diameter in UMTF atomization at 105 m/s air velocity, 2.2 mA/mL, and 3.5 W. In contrast, an aqueous jet of 0.07 wt. % PEO with the same molecular weight (2×10^6) and a lower viscosity (1.9 cSt) did not atomize at these conditions. Instead, it broke up into big drops at 6.0 W; the resulting obscuration was too low to obtain a size distribution using the Malvern particle sizer. Furthermore, as shown in Figure 13b, the drop-size distributions obtained in UMTF atomization of aqueous solutions ($\nu = 2.2$ cSt) of PEO with a lower molecular weight (2×10^5) at much more severe conditions are much broader. Thus, due to the elasticity of the Xan solutions, the absorbed ultrasonic energy that sets up the capillary waves is stored and facilitates breakup of these capillary waves upon subsequent air impingement. To the best of our knowledge, this is the first experimental evidence that elasticity facilitates liquid atomization in the presence of co-flowing air.

Like PEO solutions, increase in ultrasonic fundamental frequency from 54 to 110 kHz in ultrasonic and UMTF atomization of Xan solutions resulted in an increased ultrasonic power requirement (4.0 vs. 2.5 W at 100 m/s air velocity and 3.3 mA/mL, for example). The peak diameter obtained in UMTF atomization of 0.1 wt. % Xan solution was found to be only slightly smaller (35 vs. 40 μm) at 110 kHz than at 54 kHz; those for the 0.15 wt. % Xan solutions were identical. This lack of change in peak drop diameter in response to increases in ultrasound frequency f differed from the Newtonian behavior of $f^{-2/3}$-dependency (Tsai et al., 1996). Unlike PEO solutions, ultrasonic atomization of Xan solutions does not yield large drops with diameter greater than 200 μm, as shown in Figure 14b. Again, this may be due to network formation (or gelation) in Xan solutions. Since the Xan molecules with 2×10^6 MW are interconnected in the solution, they are not free to move as the PEO-10^5 MW molecules do. As a result, relaxation of the Xan solution occurs on a time-scale on the order of seconds, and the resulting long waves are stable in ultrasonic atomization.

Conclusion

Flow visualization of the sprays of aqueous glycerol and dilute solutions of PEO-10^5 MW demonstrates that capillary waves are initiated by ultrasound at the nozzle tip in both ultrasonic and ultrasound-modulated two-fluid (UMTF) atomization. As it travels downstream in the direction of the airflow, the capillary wave is amplified by air blowing around it. Atomization occurs when the amplitude becomes too great to maintain wave stability. The resulting drop sizes and size distributions are determined by the relative amplitude growth rates of the capillary waves at different wavelengths.

Both polymer molecular weight and molecular structure have very significant effects on the drop-size and size distribution in both ultrasonic and UMTF atomization. With polymer molecular weights (MW) up to 2×10^4, polyethylene oxides (PEO) solutions behave as Newtonian liquids in accordance with the modified Taylor's dispersion relation. As PEO molecular weight increases to 10^5, the drop-size distribution becomes broader and the peak drop diameter becomes larger because the capillary waves generated by the harmonics of the ultrasound become more comparable in amplitude growth rates. Interestingly, both drop-size analysis and high-speed flow visualization of ultrasonic atomization of the dilute solutions of PEO-10^5 MW show drops 400 ± 25 μm in diameter, which is considerably larger than the 80 μm-diameter predicted for Newtonian liquids at the fundamental ultrasound frequency of 54 kHz. The presence of these large drops may be indicative of molecular relaxation time on the order of 10^{-4} s.

More importantly, aqueous solutions of xanthan gum (Xan) with a molecular weight of 2×10^6 require much less severe aerodynamic conditions than Newtonian liquids in UMTF atomization at a fundamental frequency of 54 kHz to yield uniform drops with a peak diameter determined by the third harmonic frequency. This finding is due to the elasticity of the Xan solutions that form gel via intermolecular hydrogen bonding and runs contrary to notions that viscoelastic liquid jets are more stable than Newtonian liquid jets. The elasticity allows storage of the absorbed ultrasonic energy, which facilitates breakup of the ultrasound-generated capillary waves upon subsequent air impingement. These findings potentially have important implications for the creation of uniform drops or particles in spray coating and microelectronic processing.

Acknowledgments

Support of this work by the National Science Foundation under grant no. CTS-9812050 in the Division of Chemical and Transport System is gratefully acknowledged. The authors also would like to acknowledge the assistance of Patrick Tam and Sylvia Tsai.

Literature Cited

Berger, H. L., ''Characterization of a Class of Widely Applicable Ultrasonic Nozzles,'' ILLASS, (1985); Sono-Tek brochure (Milton, NY), ''Ultrasonic Atomizing Nozzle Systems,'' (1991).

Bird, R. B., R. C. Armstrong, and O. Hassager, ''The General Linear Viscoelastic Fluid,'' *Dynamics of Polymeric Liquids*, Vol. I, Chapter 5, Wiley, New York p. 255 (1987).

Bogy, D. B., ''Drop Formation in a Circular Liquid Jet,'' *Ann. Rev. Fluid Mech.*, **11**, 207 (1979).

Bousfield, D. W., R. Keunings, G. Marrucci, and M. M. Denn, ''Nonlinear Analysis of the Surface Tension Driven Breakup of Viscous Filaments,'' *J. Non-Newtonian Fluid Mechanics*, **21**, 79 (1986).

Chao, K. K., C. E. Child, E. A. Grens, and M. C. Williams, ''Antimisting Action of Polymeric Additives in Jet Fuels,'' *AIChE J.*, **30**, 111 (1984).

Dontula, P., C. W. Macosko, and L. E. Scriven, ''Model Elastic Liquids with Water-Soluble Polymers,'' *AIChE J.*, **44**, 1247 (1998).

Elrod, S. A., B. Hadimioglu, B. T. Khuri-Yakub, E. G. Rawson, E. Richley, C. F. Quate, N. N. Mansour, and T. S. Lungren, ''Nozzleless Droplet Formation with Focused Acoustic Beams,'' *J. of Applied Physics*, **65**, 3441 (1989).

Jeffreys, H., ''On the formation of Water Waves by Wind,'' *Roy. Soc. Proceedings*, Series A, Vol. 107, 189 (1925).

Lal, A., and R. M. White, ''Micromachined Silicon Ultrasonic Atomizer,'' *Proc. of IEEE Ulrasonics Symp.*, 339 (1996).

Lang, R., ''Ultrasonic Atomization of Liquids,'' *J. of the Acoustic Soc. of America*, **34**, 6 (1962).

Munn, R. P., B. W. Young, and D. V. Boger, ''Atomization of Dilute Polymer Solutions in Agricultural Spray Nozzles,'' *J. Non-Newtonian Fluid Mech.*, **83**, 163 (1999).

Ortiz, M., D. De Kee, and P. J. Carreau, ''Rheology of Concentrated Poly-(ethylene oxide) Solutions,'' *J. Rheology*, **38**, 519 (1994).

Pal, R., ''Oscillatory, Creep and Steady Flow Behavior of Xanthan-Thickened Oil-in-Water emulsions,'' *AIChE J.*, **41**, 783 (1995).

Peng, S. T., and R. F. Landel, ''Rheological Behavior of Progressively Shear-thickening Solutions,'' *J. Apply. Phys.*, **52**, 5988 (1981).

Rayleigh, ''On the Maintenance of Vibrations by Forces of Double Frequency,'' *Phil. Mag. S.*, **5**, **24** (# 147), 146 (1887).

Smolinski, J. M., E. Gulari, and C. W. Manke, ''Atomization of Dilute Polyisobutylene/Mineral Oil Solutions,'' *AIChE J.*, **42**, 1201 (1996).

Taylor, G. I., Generation of Ripples By Wind Blowing Over A Viscous Fluid,'' *The Scientific Papers of G. I. Taylor*, **III**, 244 (1940).

Tsai, S. C., P. Childs, P. Luu, and C. S. Tsai, ''Ultrasound-Modulated Twin-Fluid Jet Atomization,'' *Proc. of IEEE Ultrasonics Symp.*, 1085 (1995).

Tsai, S. C., P. Childs, and P. Luu, ''Ultrasound-Modulated Twin-Fluid Jet Atomization of a Water Jet,'' *AIChE J.*, **42**, 3340 (1996).

Tsai, S. C., ''Ultrasonic-Modulated Two-Fluid Atomization,'' US Patent No. 5,687,905, (Nov. 18, 1997).

Tsai, S. C., P. Luu, P. Childs, A. Teshome, and C. S. Tsai, ''The Role of Capillary Waves in Two-Fluid Atomization,'' *Phys. of Fluids*, **9**, 2909 (1997).

Tsai, S. C., P. Childs, P. Luu, and C. S. Tsai, ''Ultrasound-Modulated Two-Fluid Atomization of a Viscous Liquid Jet,'' *IEEE Trans. on Ultrasonics, Ferroelectrics and Frequency Control*, **46** (1999a).

Tsai, S. C., P. Luu, P. Tam, G. Roski, and C. S. Tsai, ''Flow Visualization of Taylor-mode Breakup of a Viscous Liquid Jet,'' *Phys. of Fluids*, **11**, 1331 (1999b).

Manuscript received Apr. 2, 1999, and revision received Jan. 6, 2000.